

Article

Winter Wheat Green-up Date Variation and its Diverse Response on the Hydrothermal Conditions over the North China Plain, Using MODIS Time-Series Data

Linghui Guo ^{1,2}, Jiangbo Gao ^{3,*}, Chengyuan Hao ¹, Linlin Zhang ^{3,4}, Shaohong Wu ^{3,4} and Xiangming Xiao ² 

¹ School of Surveying and Land Information Engineering, Henan Polytechnic University, Jiaozuo 454000, China

² Department for Microbiology and Plant Biology, Center for Spatial Analysis, University of Oklahoma, Norman, OK 73019, USA

³ Key Laboratory of Land Surface Pattern and Simulation, Institute of Geographic Sciences and Natural Resources Research, Chinese Academy of Sciences, 11A Datun Rd., Beijing 100101, China

⁴ University of Chinese Academy of Sciences, Beijing 100049, China

* Correspondence: gaojiangbo@igsnr.ac.cn

Received: 8 May 2019; Accepted: 26 June 2019; Published: 4 July 2019



Abstract: Vegetation phenology plays a critical role in the dynamic response of terrestrial ecosystems to climate change. However, the relationship between the phenology of winter wheat and hydrothermal factors is inadequate, especially in typical agricultural areas. In this study, the possible effects of pre-season climate changes on the green-up date (GUD) of winter wheat over the North China Plain (NCP) was investigated, using the MODIS EVI 8-day time-series data from 2000 to 2015, as well as the concurrent monthly mean temperature (T_m), mean maximum (T_{max}) and minimum temperature (T_{min}) and total precipitation (TP) data. Firstly, we quantitatively identified the time lag effects of winter wheat GUD responses to different climatic factors; then, the major driving factors for winter wheat GUD were further explored by applying multiple linear regression models. The results showed that the time lag effects of winter wheat GUD response to climatic factors were site- and climatic parameters-dependent. Negative temperature effects with about a 3-month time lag dominated in most of the NCP, whereas positive temperature effects with a zero-month lag were most common in some of the southern parts. In comparison, total precipitation had a negative zero-month lag effect in the northern region, but two lagged months occurred in the south. Regarding the time lag effects, the explanation power of climatic factors improved relatively by up to 77%, and the explanation area increased by 41.20%. Additionally, change in winter wheat GUD was primarily determined by temperature rather than by TP , with a marked spatial heterogeneity of the T_{max} and T_{min} effect. Our results confirmed different time lag effects from different climatic factors on phenological processes in spring, and further suggested that both T_{max} and T_{min} should be considered to improve the performance of spring phenology models.

Keywords: winter wheat; green-up date; hydrothermal conditions; North China Plain

1. Introduction

The North China Plain (NCP) is one of the world's major winter wheat production areas, accounting for approximately three quarters of the total wheat production in China, and about one eighth of the global wheat production [1–3]; it is therefore of importance for both Chinese and global food security.

However, the monsoon climate makes it sensitive to global climate change. Numerous previous studies have indicated that the climate of the NCP experienced abrupt warmer and drier spells in the past decades, and that is projected to continue in the future [4–6]. Zhang et al. [7] noted that the mean annual temperature in some parts of the NCP had increased rapidly, by 0.57–0.44 °C/10a, from 1981–2011, higher than the corresponding national and global average warming [8]. Duo et al. [9] and Wang et al. [10] suggested that the changes in temperature differed greatly among seasons and max–min temperatures, with the largest warming rate being for spring and nighttime. In comparison, although its annual precipitation exhibited larger variations over the years as a whole [9], its seasonal and regional reduction seemed to be significant [11,12]. These changing hydrothermal conditions have inevitable consequences on winter wheat growing activity [13–15]. Thus, quantifying winter wheat growth dynamics and understanding the driving mechanisms behind these variations are scientific issues of great concern.

The vegetation green-up date (GUD) plays an essential role in biosphere–atmosphere interactions, due to its strong impact on the growing season length, carbon uptake, and energy exchange [16–18]. Monitoring GUD changes in cropland could not only enhance our understanding of crop response mechanism to environments, but could also help in devising adaptive management strategies. Based on ground observation and crop model, a substantial number of studies explored the spatial temporal variation of winter wheat GUD in NCP and its influence factors [19–22]. For example, Zhou et al. [19] successfully applied digital camera images to monitoring winter wheat GUD in order to optimize an ecological model in Yucheng station. Xiao et al. [20] and Tao, et al. [21] demonstrated that the advance of winter wheat GUD in some stations was dependent upon temperature change. However, such approaches are, to a large extent, limited by the number of observation sites, and thus, are almost impossible to apply to entire regions [23].

Remote sensing data with the larger spatial coverage and higher observation frequency have been involved in identifying winter wheat GUD variation in NCP recently [23–27]. Yet, there are still some limits in previous studies. First of all, although the winter wheat land cover data was considered for many of them, winter wheat area changes during the study period need more attention, because spectral signals from other land use types and other crop species may significantly impact satellite-derived GUD variations of winter wheat [26,28]. Secondly, increasing studies have found that the responses of winter wheat GUD to climate have a certain time lag [23,27]. However, the spatial patterns for the time lag effects of winter wheat GUD responses to climate and corresponding driving factors remain unknown. Furthermore, it has been widely suggested that asymmetric warming may affect vegetation growth differentially [29–31]. Piao et al. [32] found that the leaf unfolding date variations were triggered more strongly by maximum temperatures than by minimum temperatures in the northern hemisphere. Shen et al. [33] revealed that changes in temperate grassland GUD were more strongly related to maximum temperatures than minimum temperatures in winter, but were more controlled by minimum temperatures in spring. However, very few studies have been conducted on the response of winter wheat GUD to asymmetric warming in this region.

In this study, we employed the EVI data from the MODIS and meteorological data to assess the variation of winter wheat GUD in the NCP, and to analyze diverse responses under changing hydrothermal conditions. The objectives of this study are: 1) to investigate the spatiotemporal pattern of winter wheat GUD during 2001–2015, 2) to quantify the time lag effects of climate factors on the variation of winter wheat GUD and illustrate its relative contribution, and 3) to identify the major driving factors of climate on winter wheat GUD variation.

2. Materials and Methods

2.1. Study Area

The study area is located in the NCP (31°51′–40°32′N, 110°14′–122°45′E), covering two municipalities (Beijing and Tianjin) and six provinces (Shandong, Hebei and Henan, Shanxi, Anhui and

Jiangsu) (Figure 1). It is the largest agricultural area in China, and is commonly covered by a winter wheat–maize/cotton double cropping system [34]. Winter wheat in this region, generally, is sown in late September to early October, and starts to grow before entering a dormant stage when the temperature drops in the winter. With rising temperatures in spring, the plant enters the green-up stage as leaves rapidly turn green before harvesting in the early summer. The winter wheat life cycle spans about 230 to 260 days.

2.2. Data

MODIS time series vegetation index data: To provide more available points in winter wheat growth, we used 8-day EVI data with 500 m spatial resolution from 2000 to 2015, which was obtained from the center for Spatial Analysis, University of Oklahoma. These data were derived from the MOD09A1 C6 500 m 8-day land surface reflectance data. The Best Index Slope Extraction algorithm was used to detect and remove the lower values affected by bad conditions [35], while a SG filter was used to smooth the EVI after gap-filling [36]. These data have been widely used to monitor global environmental changes [37,38].

Cropland maps with 1-km spatial resolution: A 1 km agriculture land map for 2000 and 2015 was obtained from the Resources and Environment Data Center, Chinese Academy of Sciences (<http://www.igsnr.cas.cn>) [39].

Meteorological data: Meteorological data during 2000–2015 were collected from the China Meteorological Data Sharing Service system (<http://data.cma.cn/>) [40], which provided monthly mean air temperature (T_m), mean maximum air temperature (T_{max}), mean minimum air temperature (T_{min}) and total precipitation (TP) data for 604 meteorological stations in China. Based on Digital elevation model (DEM) data, the original meteorological data was interpolated to a 1-km spatial resolution dataset using the AUSPLINE. Finally, the EVI data and land use map were resampled in accordance with monthly meteorological data using the ArcGIS software.

In situ data on winter wheat GUD: Historical observation of winter wheat GUD data for the period of 2001–2009 was recorded at the national agro–meteorological stations, and was maintained by the Chinese Meteorological Administration [13,14,23]. In practice, although winter wheat GUD is defined as the date when leaves begin to turn green after winter dormancy and the length of the new leaves reaches 1–2 cm, it is difficult to accurately determine the date of this occurrence, especially with large spatial coverage [23,25,26]. Therefore, only the stations with winter wheat GUD records between the day of the year (DOY) 30 and 140, and which were located near the winter wheat cultivating pixels derived from 2.3 section were selected. We finally obtained data from 11 agro-meteorological stations in the NCP, which contained 99 GUD records for winter wheat (Figure 1).

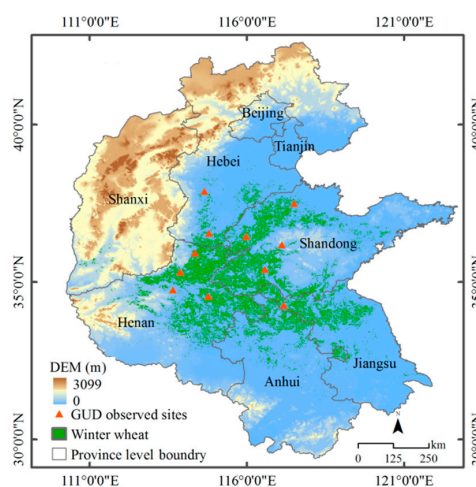


Figure 1. The spatial distribution of winter wheat cropland and eleven agro-meteorological stations in the North China Plain, China.

2.3. Identifying Winter Wheat Cropland

To focus on the areas with winter wheat, pixels were extracted by further analysis if they matched the following criteria (Figure S1). First, to reduce the impacts associated with land use change, images of the 1 km agricultural land for 2000 and 2015 were masked upon each other. Then, the remaining agricultural land was used to further mask the EVI time series data. Second, areas with sparse vegetation with EVI values no greater than 0.05 from January to February (i.e., the main winter wheat dormant stage) were excluded from the analyses. Third, a continuous smooth EVI time series data from late October to the following early July for each year over the remaining pixel was reconstructed using a sixth-order polynomial function, which was proved to effectively preserve primary curvatures while smoothing out noises [41,42]. Then, based on the sixth-order polynomial smooth EVI, pixels were further removed by applying the second order difference method [43], according to the peak (November to January)-valley-peak (April to May)-valley (May to June) patterns of winter wheat growth (Figure S2) [44]. However, given the relatively large spatial span along the NCP, it is possible that such winter wheat pixels with an unobvious first peak and valley could be excluded [44,45]. Therefore, for the single peak (April to May) pixels of the sixth-order polynomial smooth EVI, we also calculated the maximum value of the 8-day interval EVI before the sixth-order polynomial fit during November to December; as such, the pixels were selected as winter wheat cultivating zones only if the resulting value was larger than that of late October. Finally, winter wheat cultivating zones were identified by successive plantation pixels during the period of 2000–2015. The winter wheat cultivating zones matched well with the statistics yearbook area in this major winter wheat province, with general relative errors being lower than 20% (Table 1). Differences may be partly attributed to the influence of mixed pixels of MODIS EVI at 1-km resolution, and to the challenges of clarifying winter rape and winter wheat, although winter wheat is among the most widely grown crops in the NCP [26,28,44]. Additionally, 2000 random points were generated based on the agricultural land from the agricultural land 2000 map masked onto the agricultural land 2015 map, located at the center of each pixel using ArcGIS software (Figure S3). We then converted the 2000 random points to grid data with the same spatial resolution as the winter wheat extraction data. As some historical high resolution satellite images from Google Earth were not available in the key identification period of winter wheat over the whole study area, we finally selected a larger sample transect across five provinces in the study area using the available images from Google Earth for November 2014 to February 2015 to compare them with the winter wheat extraction data in 2015 (Figure S3). After that, we checked each sample grid in the sample transect with high resolution satellite images from Google Earth and the Landsat 8 surface reflection data on Google Earth Engine (Figure S4), by defining winter wheat as the sample grid area covered by $\geq 40\%$ winter wheat through visual interpretation. Sample grids without clear land cover information were excluded (22 grids). Finally, a total of 466 grids were generated for the validation of resultant winter wheat extraction data, including winter wheat (290 grids) and non-winter wheat (176 grids). A confusion matrix of the winter wheat map was calculated to evaluate the accuracy of the results [46]. The validation indicated that the winter wheat extraction data had relative high accuracy, i.e., 86% (Table 2).

Table 1. Comparison between the winter wheat cultivating zones from EVI and that from statistics yearbook in major winter wheat province.

Region	Statistical Area 10 ³ hm ²			Extraction Area 10 ³ hm ²			Relative Error %		
	2001	2007	2015	2001	2007	2015	2001	2007	2015
Hebei	2579.80	2412.40	2318.87	2491.90	2306.90	2595.60	−3.41	−4.37	11.93
Henan	4801.60	5213.33	5425.66	3984.20	4504.40	5029.20	−17.02	−13.60	−7.31
Shandong	3545.75	3519.08	3799.83	4098.10	3755.50	4098.40	15.58	6.72	7.86
Anhui	1742.72	2330.27	2457.00	1650.80	2065.10	2587.60	−5.27	−11.38	5.32
Jiangsu	1712.81	2039.12	2178.83	2530.20	1842.10	1938.80	47.72	−9.66	−11.02

Table 2. Confusion matrix of land cover validation based on sample grids from high resolution satellite images from Google Earth and from the Google Earth Engine.

Class	Winter Wheat	Non-Winter Wheat	Classify Total	User Accuracy	Producer's Accuracy	Overall Accuracy
Winter wheat	281	54	335	0.84	0.97	0.86
Non-winter wheat	9	122	131	0.93	0.69	
Sample total	290	176	466			

2.4. Estimating Winter Wheat GUD

We employed the four-parameter logistic function, which has been extensively used to determine vegetation GUD and is considered reliable [27,47], to fit a cumulative EVI time series and to determine the maximum curvature with which to derive the GUD. In addition, previous studies have exhibited that GUD extraction was usually sensitive to the vegetation index curve [24,48,49]. Therefore, firstly, we did not artificially define a yearly winter wheat EVI curve ending in July like Wang et al. [23], but rather, we set it as the DOY of the minimum EVI occurring from May to early July. Subsequently, we calculated the minimum EVI value before the maximum EVI value from the start of a year to July, which was used to replace the EVI values before the minimum EVI happened, to eliminate as much as possible the influence from summer crop EVI and spring disturbances (e.g., spring snow, dormancy delay) on winter wheat EVI curve. The winter wheat GUD extraction steps are described below:

For each year, we first calculated the *cumEVI* for 8-day interval EVI using Equation (1). Then, a four-parameter logistic function was employed to fit the *cumEVI* data to retrieve the winter wheat phenology [Equation (2)]. Finally, winter wheat GUD was defined as the day when the curvature of the fitted four-parameter logistic *cumEVI* curve reached its maximum [Equation (3)] (Figure 2).

$$cumEVI_t = \sum_{i=1}^t EVI_i \quad (1)$$

$$cumEVI_t = \frac{c}{1 + e^{a+bt}} + d \quad (2)$$

$$K = -\frac{b^2 cz(1-z)(1+z)^3}{[(1+z)^4 + (bcz)^2]^{3/2}} \quad (3)$$

where t represents DOY for 8-day interval; $cumEVI_t$ is the cumulative EVI from 1 DOY to time t ; a and b are fitting parameters, the sum c and d is the maximum *cumEVI*, and d is the minimum *cumEVI*; K represents the curvature, $z = e^{(a+bT)}$; T is DOY on a daily scale.

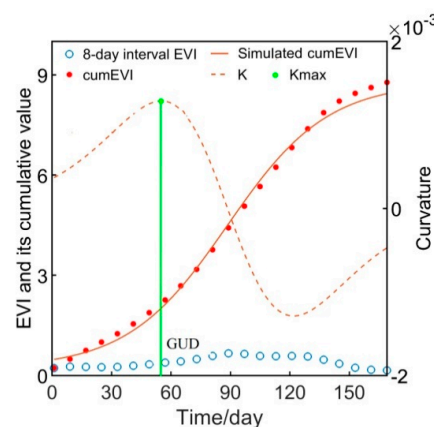


Figure 2. Illustration of winter wheat GUD extraction. K represents the curvature of the fitted *cumEVI*. K_{max} indicates the maximum of K .

2.5. Statistical Analysis

To evaluate the performances of winter wheat GUD extraction, winter wheat GUD observations data and the corresponding average GUD from 17×17 pixels around the center of each ground station for a given year were analyzed. The determination coefficient (R^2), root mean square error (RMSE) and difference between estimations and observations (Bias) were calculated. The temporal trends in winter wheat GUD from 2001 to 2015 were estimated on pixel and regional scales using linear regression.

The time lag effects of winter wheat GUD response to climatic factors included two sections; the first was the time lag response based on the Windowed Cross Correlation (WCC) method [50,51]; the second was the correlation between climate factors and winter wheat GUD according to the Pearson correlation coefficient. In accordance with the studies of Wu et al. [51] and Wen et al. [52], we limited the lagged time range to zero to three months before the month of occurrence of the multiannual mean winter wheat GUD at the regional and pixel scales, respectively. Moreover, to investigate the time lag effects of climatic factors on winter wheat GUD, we first calculated the first-difference time series (i.e., the value of every year minus the value in the first year) for winter wheat GUD (ΔGUD) and the corresponding climate factors ($\Delta T_m, \Delta TP, \Delta T_{min}, \Delta T_{max}$) to get rid of non-climatic influences, such as crop management [53,54].

The WCC model is as follows:

$$\Delta GUD = k_n * \Delta T_{m(n)} + \varepsilon \quad (0 \leq n \leq 3) \quad (4)$$

$$\Delta GUD = k_n * \Delta TP_{(n)} + \varepsilon \quad (0 \leq n \leq 3) \quad (5)$$

$$\Delta GUD = k_n * \Delta T_{min(n)} + \varepsilon \quad (0 \leq n \leq 3) \quad (6)$$

$$\Delta GUD = k_n * \Delta T_{max(n)} + \varepsilon \quad (0 \leq n \leq 3) \quad (7)$$

$$T_{lag} = n, \text{ when } R_n^2 = \max(R_0^2, R_1^2, R_2^2, R_3^2) \quad (0 \leq n \leq 3) \quad (8)$$

For each climate factor, T_{lag} is the lagged time interval, and k_n and R_n^2 are the regression coefficients and highest determination coefficients of regressions for the different lagged time range, respectively. n represents the previous months ranging from 0 to 3, marked separately for T0, T1, T2, T3. $\Delta T_{m(n)}, \Delta TP_{(n)}, \Delta T_{min(n)}, \Delta T_{max(n)}$ refers to the first-difference time series of TP and average T_m, T_{min}, T_{max} with pre n months, respectively. For instance, $\Delta T_{m(2)}$ refers to the first-difference time series of the average T_m from the current month to the previous two months.

Finally, we developed a multiple linear regression model between the normalized ΔGUD and $\Delta TP_{(n)}, \Delta T_{min(n)}, \Delta T_{max(n)}$ to determine the asymmetry temperature and precipitation variation on winter wheat GUD variation.

$$s\Delta GUD = A_n * s\Delta T_{max(n)} + B_n * s\Delta T_{min(n)} + C_n * s\Delta TP_{(n)} + \varepsilon \quad (9)$$

where $s\Delta GUD, s\Delta T_{max(n)}, s\Delta T_{min(n)}$ and $s\Delta TP_{(n)}$ refer to normalized $\Delta GUD, \Delta TP_{(n)}, \Delta T_{min(n)},$ and $\Delta T_{max(n)}$ are based on the min-max normalization method, respectively. A_n, B_n and C_n are the regression coefficient values for different climate factors. The regression with the highest determination coefficient among the different previous months was chosen as the best fit, and the corresponding regression coefficient was considered as the impact of the corresponding climate variable on winter wheat GUD; the larger the absolute value, the stronger the influence. Finally, all of the statistical analyses were performed at a significance level of 0.05 and 0.10.

3. Results

3.1. Comparison of Winter Wheat GUD Derived from MODIS Data and In-situ Data at Selected Sites

As shown in Figure 3, the satellite-derived GUD was significantly correlated with the 99 field-observed GUD from eleven agro-meteorological stations in the period of 2001–2009, with a determination coefficient of 0.30 ($P < 0.01$). The Bias and RMSE values were approximately 13 days and 12.3 days, respectively, which indicates that the satellite-derived GUD slightly overestimated the field-observed GUD.

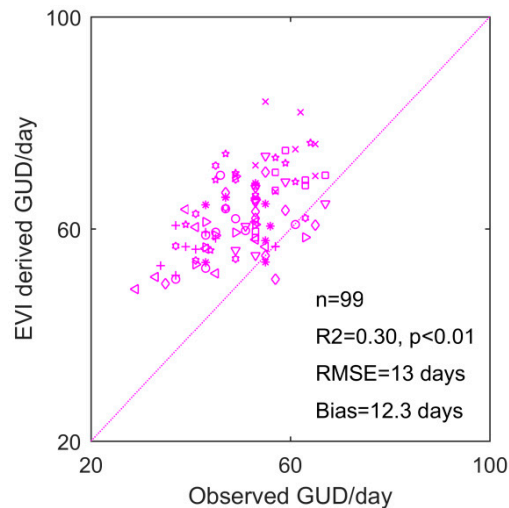


Figure 3. Validation of the satellite-derived GUD in relation to the field-observed GUD. The red dashed line is the 1:1 relationship, and the various symbols represent the eleven agro-meteorological stations.

3.2. Spatial-temporal Trends of Winter Wheat GUD

3.2.1. Spatial Patterns

Multiyear average winter wheat GUD displayed clear spatial variations, with the onset of multiyear mean GUD mostly occurring in mid-February to early-March (Figure 4a). Generally, early GUD was found in the southwest region of the NCP, whereas later arrivals of GUD occurred mainly in the northeastern part. The regions with GUD from DOY 50 to 60 accounted for approximately 46.84% of all pixels, which were widely distributed in the southern area of the NCP. A similar southwest to northeast trend was also found in the standard deviations of GUD, which were generally between 6 and 9 days (63.36%), except for some lower values in the southeast parts. Additionally, a significantly positive relationship between the multiyear average GUD and the local latitude at one-degree intervals was detected on the regional scale, which revealed that the onset of GUD occurs 2.65 days later for each 1° rise in latitude (Figure 5). Moreover, the multiyear mean GUD was shown to be significantly related with the local elevation at 100-m steps, indicating that for every 1000 m increase in elevation, the advent of GUD was delayed by 0.1 days.

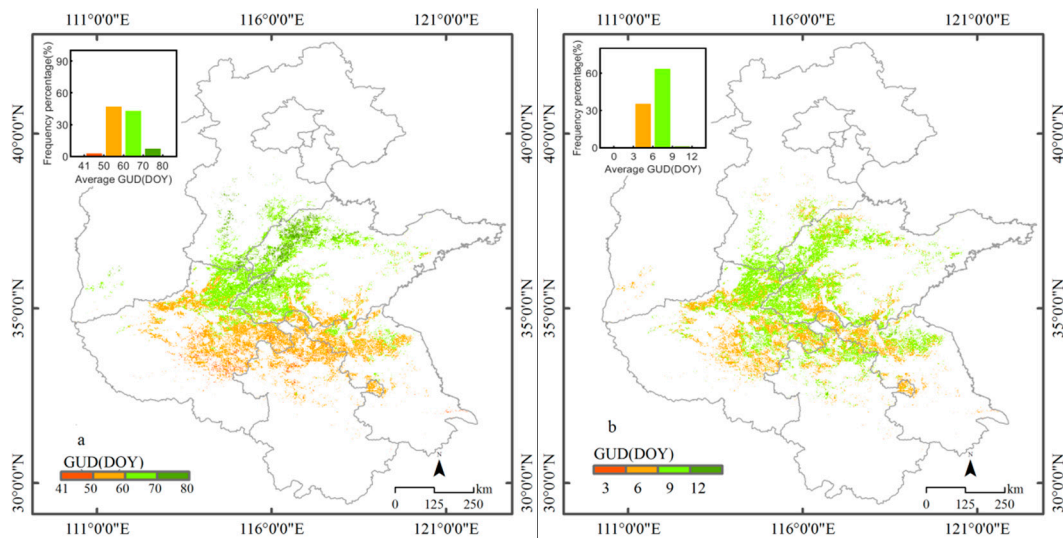


Figure 4. Spatial distribution of multiyear averaged GUD (a) and its Standard deviation (b) during the period of 2001–2015. Inset plots display the corresponding frequency distribution.

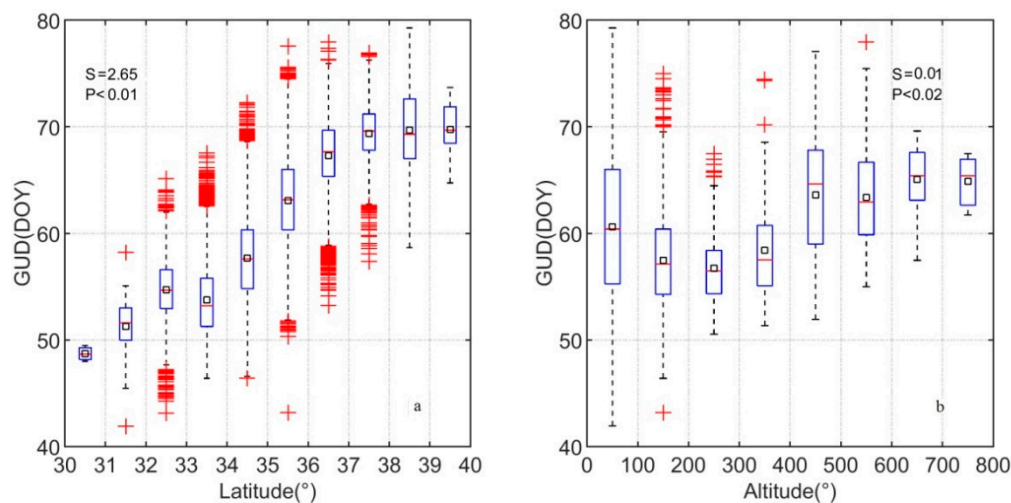


Figure 5. The latitudinal (a) and elevational (b) shifts in multiyear averaged GUD. The bottom and top edges of each blue box indicate the 25th and 75th percentiles, respectively. The horizontal red line in each blue box represents the median values. The black square in each blue box represents the mean values. The black whiskers extend to the 1.5 times the interquartile range. Red crosses mean outliers. The black texts in the upper corner present the slope (S) and significance (P) of the corresponding linear regression.

3.2.2. Variation

At a regional scale, winter wheat GUD for NCP showed no significant temporal trend (1.4 days/decade) during the period from 2001 to 2015, but sharply advanced after 2010, with an overall rate of -2.82 days/year ($P < 0.05$) (Figure 6). Spatially, the interannual variations in mean GUD for the NCP region are shown in Figure 7. It The advance of GUD was extensively observed across more than 63.57% of all pixels from 2001 to 2015, which were mainly focused on the southwest and central parts of NCP; however, most of them were not significant (Figure 7b), with about 8.62% of all pixels being statistically significant, i.e., at the $P < 0.05$ level. In contrast, areas towards the eastern parts of the NCP exhibited a notable delayed trend, accounting for 36.40% (3.20% was significant) of the total area, especially in the north part of Jiangsu Province, with GUD delayed by up to 2 days/year.

In contrast, the variation characteristic from 2010 to 2015 was also investigated in order to gain a better understanding of GUD variations. As shown in Figure 8, 98.98% of all pixels showed an advancing trend. Areas with GUD which was significantly advanced (52.03% of all pixels) mainly occurred in the southwest to northeast parts of the NCP, and these GUD advances were greater in the areas closer to the central and northeast parts of the NCP, at a rate of more than 3 days/year ($p < 0.05$). In addition, most of the southeast region experienced a slight advance, ranging from 0 to 3 days/year, but this was not significant ($p > 0.05$) (Figure 8b).

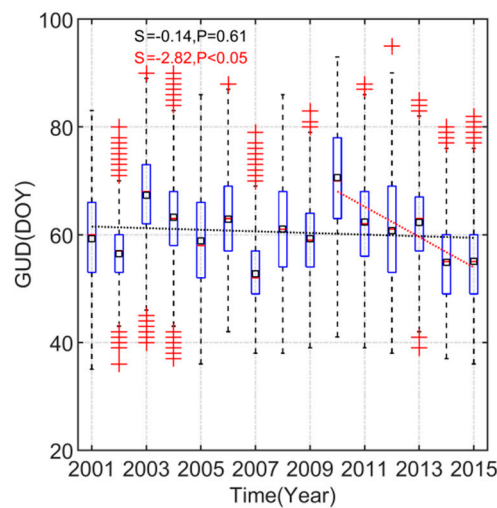


Figure 6. Interannual variations of regional GUD for 2001–2015. The bottom and top edges of each blue box indicate the 25th and 75th percentiles, respectively. The horizontal red line in each blue box represents the median values. The open black square in each blue box represents mean values. The black whiskers extend to the 1.5 times the interquartile range. Red crosses mean outliers. The black dot line is GUD trend during the period of 2001–2015, and the black texts in the upper left corner present the corresponding slope (S) and significance (P). The red dot line is GUD trend during the period of 2010–2015, and the red texts in the upper left corner present the corresponding slope (S) and significance (P).

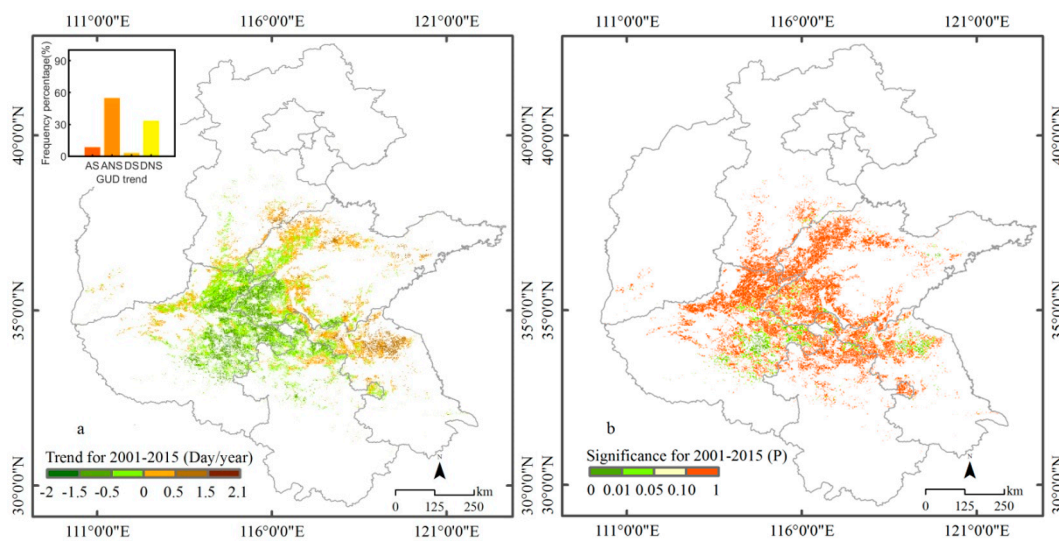


Figure 7. Spatial trends of GUD in the period 2001–2015 (a), and its significance levels (b). The inset plot presents the frequency percentage of GUD trends. AS, ANS, DS and DNS indicates advanced significantly, advanced but not significantly, delayed significantly, delayed but not significantly, at $p < 0.05$ level, respectively.

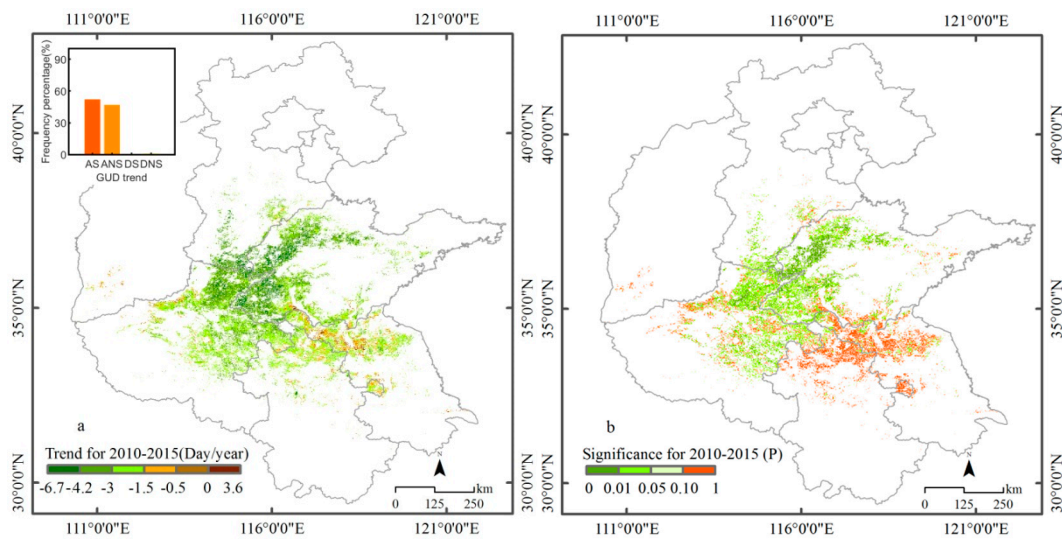


Figure 8. Spatial trends of GUD in the period of 2010–2015 (a), and its significance levels (b). The inset plot presents the frequency percentage of GUD trends. AS, ANS, DS and DNS indicates advanced significantly, advanced but not significantly, delayed significantly, delayed but not significantly, at $p < 0.05$ level, respectively.

3.3. Time Lag Effects of Winter Wheat GUD Responses to Climatic Factors

3.3.1. Interannual Variations of Climatic Factors

Figure 9 shows that the interannual trends of pre-season temperature decreased, albeit in a statistically insignificant manner, during the period of 2001–2015, but almost significantly increased during the period of 2010–2015 ($P < 0.10$). In general, during the period of 2010–2015, the pre-season T_m of T0, T1 T2 and T3 increased by 0.44 ($p = 0.05$), 0.44 ($p = 0.06$), 0.42 ($p = 0.07$) and 0.36 ($p = 0.07$) $^{\circ}\text{C year}^{-1}$, respectively. T_{min} also experienced an obvious increase in all the pre-season, at $P < 0.10$ level, with the greatest rate of 0.41 $^{\circ}\text{C year}^{-1}$ at T1, while T_{max} displayed a larger rising slope that only reached $P < 0.10$ level in T0 and T1. Moreover, for regional pre-season precipitation, it slightly decreased, mostly in the pre-season during the periods of 2001–2015 and 2010–2015, but only significantly decreased by 2.08 mm year^{-1} ($P < 0.05$) in T2 from 2001 to 2015 (Figure 9).

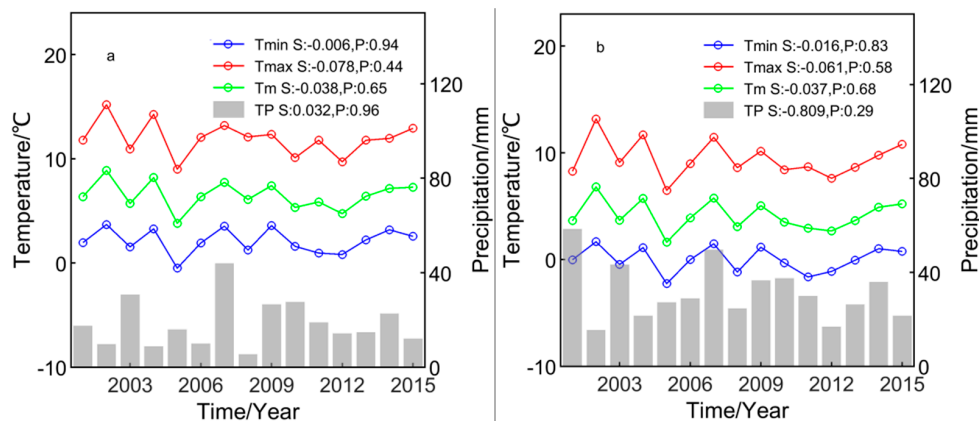


Figure 9. Cont.

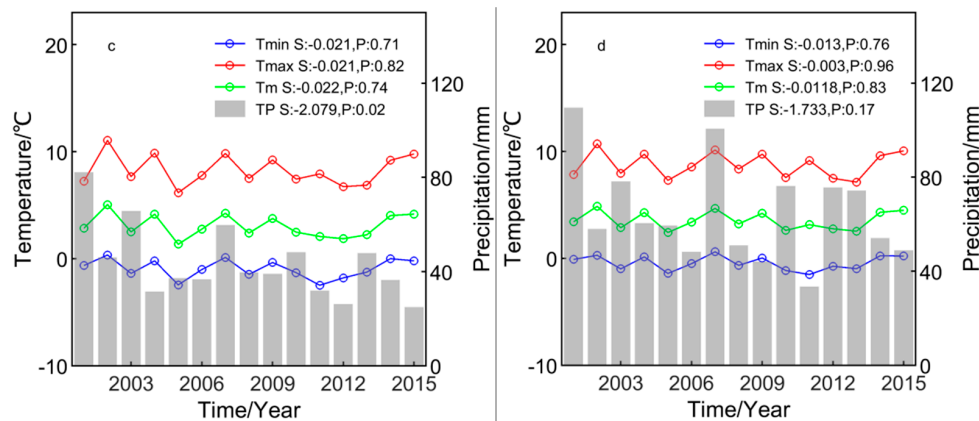


Figure 9. Variations of the different preseason T_m , TP , T_{max} , T_{min} for the winter wheat area in NCP over the study period. (a–d) indicate T0, T1, T2, and T3, respectively. The texts in the upper right corner of each figure present the slope (S) and significance (P) of the linear regression.

3.3.2. Time Lag Effect of Climatic Factors on Winter Wheat GUD

Table 3 shows the time lag effects of the winter wheat GUD responses to climate factors on a regional scale. In particular, GUD gradually reached the greatest correlation with T_m in T3, which suggests that winter wheat GUD has a 3-month lag relative to mean temperature. Similarly, there was a consistent time lag response to T_{max} and T_{min} , but the relationship between GUD and T_{max} was much stronger than that of T_{min} . Additionally, GUD did not exhibit a significant time lag effect with TP , but was slightly negatively correlated to TP in T0, and positively related with TP in T1–T3, especially in T2, indicating that the winter wheat green-up was not primarily prompted by the precipitation of the current month, but rather, that of the previous two months.

Table 3. The time lag effects of GUD responses to climatic factors for 2001–2015 on a regional scale.

Climate Factors	Determination Coefficient (R^2)			
	T0	T1	T2	T3
T_m	0.17	0.19	0.28	0.46**
TP	0.06	0.003	0.05	0.008
T_{min}	0.16	0.14	0.17	0.35*
T_{max}	0.13	0.20	0.31*	0.44**

* indicates significance at the 0.05 level, ** indicates significance at the 0.01 level.

The spatial pattern of the time lag effects of winter wheat GUD responses to the four climatic factors was shown in Figure 10. In general, the GUD for 78.57% of the total pixels showed a 3-month time lag effect related to T_m . Furthermore, 45.26% of the total area was significant, revealing that the GUD in most parts of the NCP was primarily influenced by T_m in previous months. However, in some parts of central and southern NCP, and especially in southern NCP (1.65% of all pixels were significant), the GUD did not exhibit a time lag effect to T_m , and was positively related to T_m in the same month (Figure 10a). This indicates that T_m could strongly inhibit winter wheat greening in the same month in the relatively high temperature region, possibly because temperature increases cause drought and promote soil moisture evaporation, thus inhibiting winter wheat growth.

With respect to TP (Figure 10b), the results revealed that approximately 37.41% of all pixels (8.21% of all pixels were significant) did not show time lag effects, and were negatively affected by TP , which was mainly located in the northern NCP. In the regions with relatively southern parts, the response of the GUD to TP showed there was a time lag effect of one or two months, which accounted for 23.69% and 26.29% of all pixels (3.74% and 5.26% of all pixels were significant, respectively), respectively.

In addition, similar patterns to T_m were found in the time lag effects of GUD responses to T_{min} and T_{max} . However, notably, most of the GUD in relatively central and northern areas of the NCP showed the greatest response to T_{min} in T1, making up 24.08% of all pixels, with more than 40% of them being significant (Figure 10c,d). Moreover, the time lag of winter wheat in the northern region to T_{max} was approximately 2 months. This indicated the demands of winter wheat growth for temperature increase in the relatively high latitude regions of the NCP.

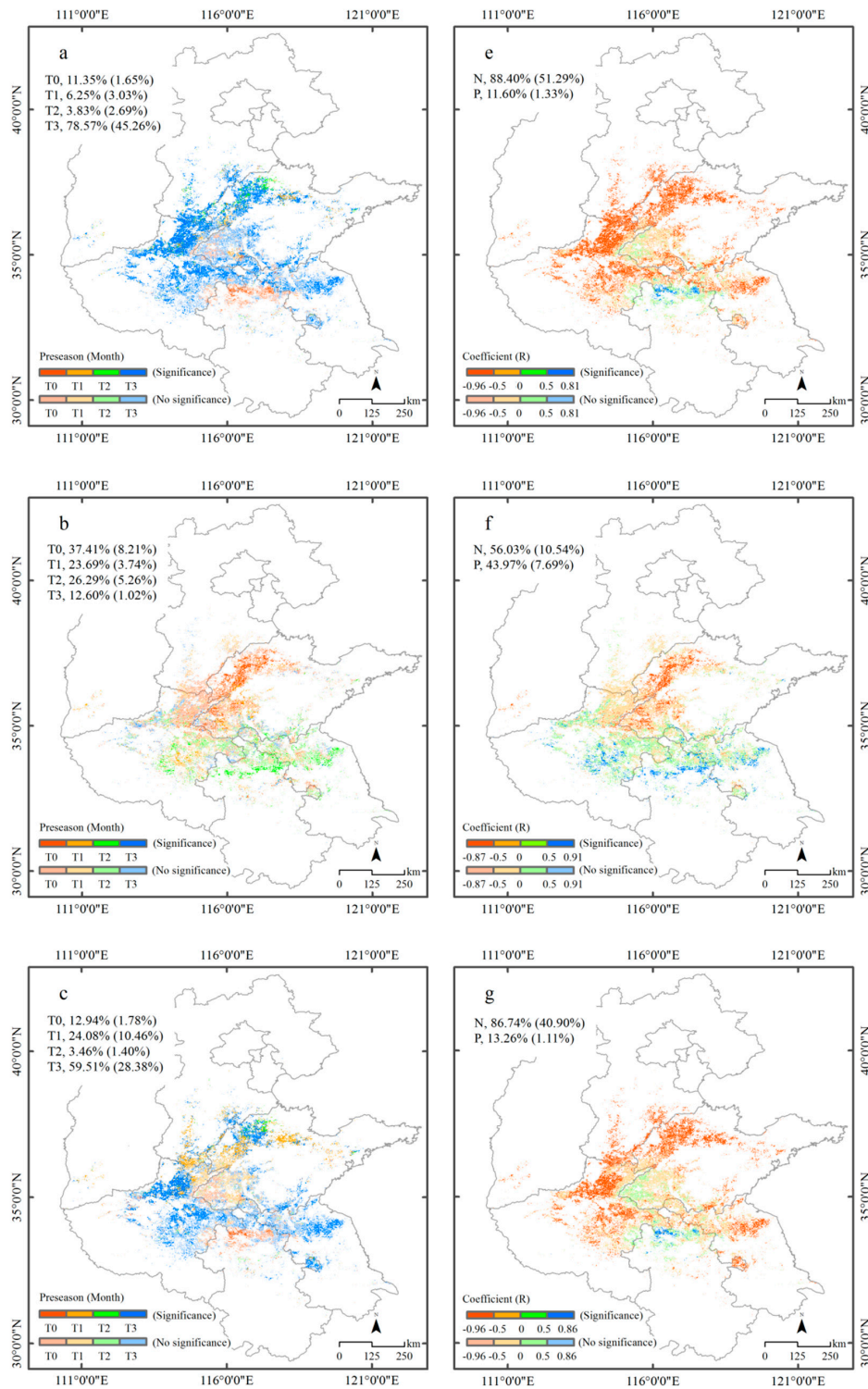


Figure 10. Cont.

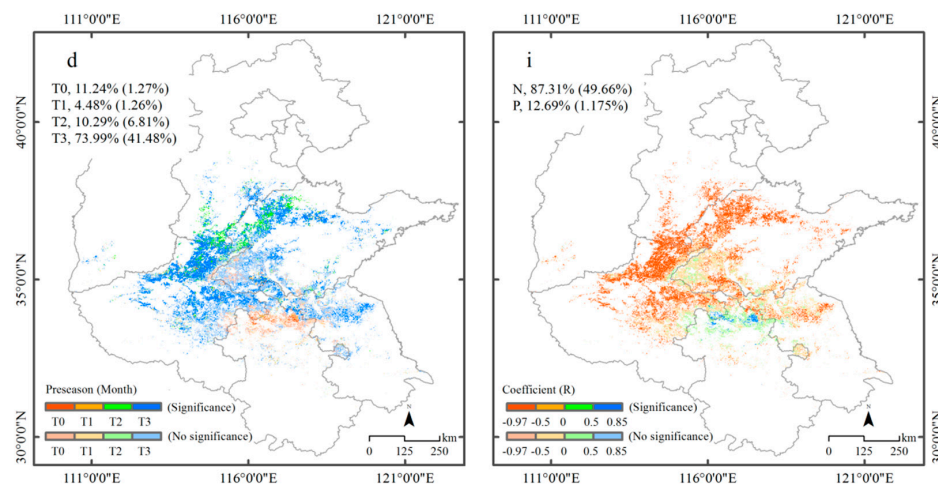


Figure 10. GUD time lag responses to T_m , T_P , T_{min} , T_{max} (a–d) and its relationship (e–i), respectively. Areas with no statistical significance ($P < 0.05$) are depicted in the corresponding color with 60% transparency. The texts in the upper left corner of each left figure present the percentage of lag time (T0, T1, T2, and T3) ($P < 0.05$, percentage of significant lag time in parentheses). The texts in the upper left corner of each right figure present the percentage of positive (P) and negative (N) correlations ($P < 0.05$, percentage of significant correlations in parentheses).

Figure 11 shows the climate contributions to winter wheat GUD by using the determination coefficients of the multiple linear regression models. The result illustrated that if the lag effect was ignored, only 39.63% of all pixels GUD could be significantly explained by the three climatic factors, i.e., those which were mainly located in north area (Figure 11a,b). However, considering the time lag effects, the explanation area increased by 41.20% (i.e., about 55.96% of the winter wheat region). On the other hand, the explanation ability of these climate factors on the GUD also improved substantially. For example, the explanation ratio increased by 0–15% over 28.25% of the pixels, by 15–30% over 9.18% of the pixels, and by more than 30% across 2.35% of the pixels, respectively (Figure 11b). This indicated that consideration of winter wheat GUD time lag effects to climatic factors are most important for modelling predictions.

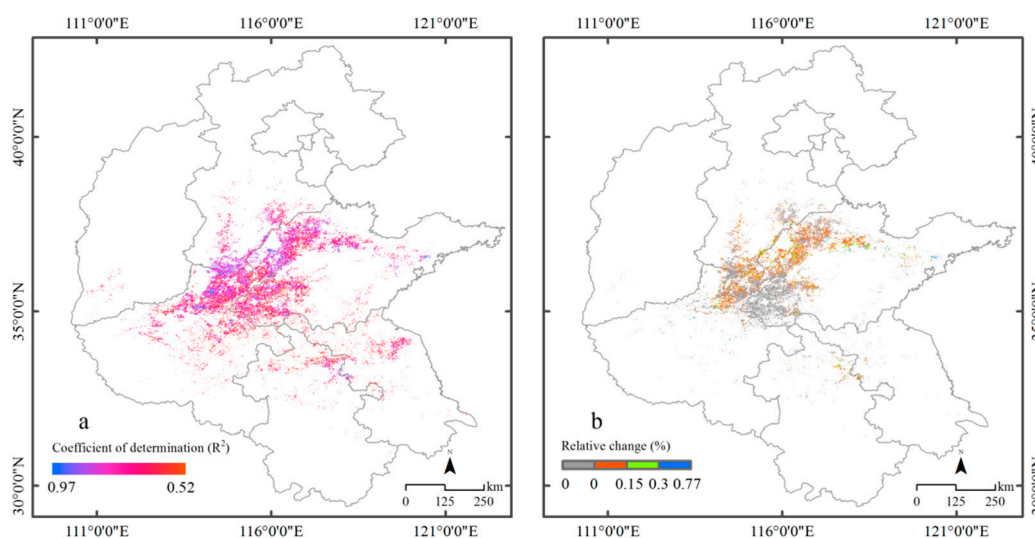


Figure 11. Spatial distribution of the determination coefficient (R^2) of the multiple linear regression model between GUD and climatic factors for the period of 2001–2015, considering time lag effects (a), and (b) its relative change compared with ignoring the time lag effects.

3.4. Driving Factors for the Spatial-Temporal Changes of Winter Wheat GUD

As pointed out previously, the winter wheat GUD advanced rapidly from 2010 to 2015. Therefore, in contrast to the above analysis, the major driving factors on winter wheat GUD variation during this period and its influence was explored as follows. As illustrated in Figure 12b, more than 50.19% of all pixels were primarily controlled by T_{max} during the period of 2010–2015, with about 15.60% of all pixels being significant ($p < 0.05$) and mainly distributed in northern central part of the NCP. In comparison, T_{min} controlled the areas mainly located in the south western and some north eastern parts of the NCP, accounting for 2.84% of all pixels ($p < 0.05$, Figure 12b). The area with GUD variation generally controlled by TP was sporadically scattered across the central and southern regions. Interestingly, the impact of TP change on GUD was negative over the central region, but positive across some of the southern part (Figure 12a).

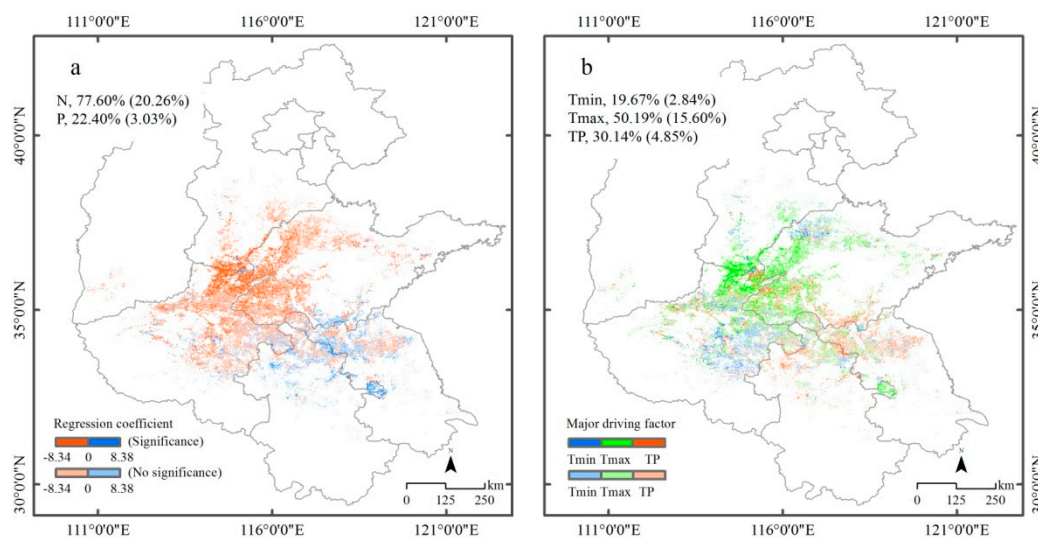


Figure 12. Spatial distribution of multiple regression coefficient between GUD and climatic factors (a) and main climate-driven factors to GUD (b) during the period of 2010–2015. Percentage of positive (P) and negative (N) correlations and corresponding significant correlations ($P < 0.05$, in parentheses) are shown in Figure 12a. Percentage of different major driving factors (T_{min} , T_{max} , and TP) controlling area and corresponding significant area ($P < 0.05$, in parentheses) are shown in Figure 12b.

4. Discussion

4.1. Winter Wheat GUD Extraction Algorithm

Our evaluation was shown to slightly overestimate the field-observed winter wheat GUD. This difference may be caused by two factors, i.e., the differences between winter wheat GUD definitions and the spatial resolution, as addressed in other studies [26,47,49]. On one hand, the field-observed winter wheat GUD is defined as the date when the leaves begin to turn green after winter dormancy, and when the length of the new leaves reaches 1–2 cm, while the satellite-derived winter wheat GUD is calculated based upon the maximum curvature, which could be later in theory. On the other hand, the determination coefficient (0.45) between the field-observed winter wheat GUD and the satellite-derived winter wheat GUD of the nearest pixel, for example, was larger than that between the field-observed winter wheat GUD and the mean satellite-derived winter wheat GUD of the near 17×17 pixels (0.19) in the Xinxiang agro-meteorological station. However, the opposite was true at the Huimin agro-meteorological station (the determination coefficients were 0.25 and 0.33, respectively); therefore, spatial heterogeneity could also result in this discrepancy. Additionally, the results exhibited a better relationship than that reported in previous studies [23,27], which was probably related to the fact that we did not artificially limit the period from January to July to calculate the cumulative EVI, instead of

the period from January to the time of minimum EVI occurring in the early summer. Of course, it could also be partly caused by the different temporal and spatial resolution [27,48]. These findings indicated that our algorithm was suitable to investigate the GUD variation for winter wheat over the NCP.

4.2. Interannual Variations of Winter Wheat GUD

It has been widely reported that the spring GUD generally advanced in temperate and cold regions in the last two decades of the twentieth century [41,42,55], specifically, by 2.8 days/decade over the Northern Hemisphere [42], 3 or 4 days/decade in Eurasia or North America [56], and 8 days/decade across temperate zone of China [41]. However, our analyses found that winter wheat GUD over the NCP revealed a slight advancing trend of 1.4 days/decade during the period of 2001–2015 ($P = 0.61$). The discrepancy may be related to the global warming slowdown in the 2000s [57–59] which was associated with the weakened spring GUD advance signals [23,41]. Another possible reason was that global warming comes with a loss of chilling, which may counteract the advance of leaf unfolding in response to warming [60,61]. Recently, Liu et al. [27] showed that winter wheat GUD of NCP was delayed by 4.3 ($P = 0.15$) or 6 ($P = 0.08$) days/decade from 1999–2013 based GIMMS NDVI and SPOT-VGT NDVI, which seemed slightly out of accordance with our result. However, the difference was partly related to the study period; if we focused on the period of 2001–2013, our estimate of winter wheat GUD variation (2.2 days delay per decade, $P = 0.53$) was a little bit lower than that of Liu et al. [27]. Additionally, this discrepancy could also be attributed to the comparison between winter wheat GUD trends with and without calibration of land use changes, and was likely caused by the spectral signal from vegetation type turnover in the time series. Therefore, careful calibration of land use and cover change impacts is necessary to reasonably estimate vegetation phenology variations.

Furthermore, our results also provided more details of winter wheat GUD changes from the recent global surface warming slowdown to the record heat in the extreme El Niño year [62]. From 2010 to 2015, a significantly widespread advance trend in winter wheat GUD appeared over most of the NCP, with a mean rate of about 4 times that of temperate zone in China in the period of 1982–1999 [41]. The dramatical GUD change highlighted the necessity for improving our mechanical understanding of the interactions between phenology and food production to ensure regional food security and to cope with climate change, because a change in spring phenology could not only influence the structure and function of the ecosystem, but could also feedback on the atmosphere [17,18].

4.3. Major Driving Factors on Winter Wheat GUD

Temperature has been widely recognized as a major climatic factor of spring vegetation GUD in temperate and boreal regions [31–33]. An increase in accumulation temperature during the pre-season may result in an advance of vegetation emergence [42]. Our results confirmed the importance of temperature in influencing winter wheat GUD. Firstly, in our study, the latitudinal shift in winter wheat GUD was a 2.65-day advance for each 1° latitudinal decrease, which was similar to the previous findings for China [26] and North America [63], where the onset of GUD exhibited a shift of 2.59 days and 2.17 per latitude degree. Secondly, accompanying an obvious increase in pre-season temperature, winter wheat GUD demonstrated significant advance, i.e., at a rate of -2.82 days/year during the period of 2010–2015. Furthermore, temperature (both T_{min} and T_{max}) was the major driving factor of winter wheat GUD, accounting for 69.86% of all pixels, with about 18.44% of all pixels being significant. However, interestingly, the asymmetric impacts of T_{min} and T_{max} on winter wheat GUD was obvious in the NCP; this may be associated with the efficient heat requirement of growing degree days, the photoperiod and the confounding effects of water availability [31,32]. Further experimental studies are needed to identify the physiological mechanisms underlying the asymmetric impacts of T_{min} and T_{max} on winter wheat GUD.

In contrast to temperature, our results also indicated that about 4.85% of winter wheat GUD was significantly dominated by pre-season precipitation, but that its impact differed among regions. For instance, the onset of winter wheat GUD over the southern area was postponed by an increase

of precipitation, whereas such precipitation appeared to cause an advanced trend for parts of the northern region. These contradictory patterns may be related to the local environment [24,27,41]. Compared with southern area in the NCP, the northern part mainly appeared under conditions of low precipitation, in which the intensity and frequency of droughts in spring and winter were the main limits for winter wheat growth [64]. On the other hand, increasing precipitation in the southern area with relatively abundant rainfall was usually accompanied by an increase in clouds, and thus, a reduction in incoming solar radiation and temperature [41]. Furthermore, it should be noted that winter wheat GUD in some areas was neither mainly determined by mean maximum or minimum temperatures nor by total precipitation, revealing that variations in winter wheat phenology are possibly driven by other environmental or agronomic factors, such as solar radiation [14], crop type, planting, and irrigation [13,15].

4.4. Diverse Time Lag Effects of Winter Wheat GUD Response

The time lag response of vegetation growth to climate change has been widely reported in terrestrial ecosystem studies [65–67]. Based on NDVI data, Wu et al. [51] found that the average explanation of climatic factors to vegetation growth will increase from 52.8% to 63.52% globally when time lag effects are considered. If the cumulative climate effect is considered, the explanatory power would be approximately 3.35% higher [52]. Similarly, our results indicated that not only the explanation ability of the three climate factors on winter wheat GUD can be relatively improved by 0–77%, but also that the explanation area could increase by 41.20% when the pre-season climate effect was considered, which suggests that vegetation phenology response studies should be improved by taking into account of the time lag effects of climatic factors on vegetation.

Moreover, our results revealed that the time lag response of winter wheat GUD to climate factors was site- and climatic parameters-dependent. In most of the NCP, winter wheat GUD was negatively determined by the mean temperature in the previous 3 months, which was consistent with previous findings [41,42,68]. However, winter wheat GUD in the middle of southern parts was mainly positively restricted by the mean temperature in the same month. Meanwhile, as illustrated in Figure 10b,f, the total precipitation had a remarkable zero-month lag effect on winter wheat GUD in the northern region, whereas a two-month lag dominated in the southern area. This situation may be the result of differences in the respective growth environments. For example, in the northern region with low precipitation and low temperatures, temperature increases in the pre-season could prompt heat accumulation to trigger spring leaf onset and enhance activities of photosynthetic enzymes, thus advancing the onset dates of vegetation green-up [32,69], but its related water stress may inhibit vegetation growth to some extent [70]. This is a possible reason why winter wheat GUD was highly positively correlated with precipitation in this region. By contrast, the relatively weaker precipitation in the previous two months (Figure S5) could reduce soil water content, which would partly or totally offset the advancing effects of temperature on the GUD in the southern area (Figure 10b,f). Additionally, further analyses showed that the time lag effects of winter wheat GUD response to maximum temperatures occurs one month earlier than that of minimum temperatures in some parts of northern NCP; this could be partly attributed to maximum rather than minimum temperatures more efficiently fulfilling the growing degree days requirement, which triggers leaf onset in early spring, when minimum temperatures are still below the threshold [32]. This result may provide valuable information that could be used to improve the performance of the current global carbon cycle models.

However, the relationship between vegetation and climate is extremely complicated owing to the non-linear responses of vegetation to climate change and their spatial heterogeneity [71–73]. Therefore, applying other approaches instead of linear regression to identify the relative contributions of climate factors on winter wheat GUD should be undertaken in the future.

5. Conclusions

In summary, we analyzed the time lag effects of winter wheat GUD responses to climatic factors using MODIS EVI 8-day data and monthly climate data from 2001 to 2015 across the North China Plain. Our results showed that no significant trend in the green-up date averaged over NCP for the period of 2001–2015, but, interestingly, we found a strongly significant advance during the period of 2010–2015, at a rate of -2.82 days/year ($P < 0.05$), with a widespread advancing trend across the southwest to northeast part of the NCP (52.03% of all pixels). The time lag response of winter wheat GUD to climate factors was site- and climatic parameters-dependent. In general, winter wheat GUD negatively responded to temperature with a time lag of about 3 months in most parts of NCP, whereas in some of southern parts, it showed a zero-month lagged response. Meanwhile, total precipitation had a remarkable zero-month lag effect on winter wheat GUD in the north region, but two lagged months dominated in the southern area. When the time lag effects of climatic factors were considered, their explanation ability significantly increased by 0–77%, and the explanation region rose by approximately 41.20%, indicating that considering time lag effects could provide a better understanding of the interactions between GUD and climatic factors. Additionally, our results confirmed the importance of temperature on winter wheat GUD, although the T_{max} and T_{min} effect showed marked spatial heterogeneity.

Supplementary Materials: The following are available online at <http://www.mdpi.com/2072-4292/11/13/1593/s1>, Figure S1. The workflow for winter wheat area identification. Figure S2. A sample of winter wheat EVI time series during growth cycle in NCP and its sixth-order polynomial smooth. Figure S3. Random points and validation sample transect for winter wheat extraction in this study. Figure S4. The true color synthesis map over the sample transect during December 2014 to January 2015 based on Landsat 8 imagery and Google Earth Engine platform. Figure S5. Spatial distribution of TP trend (a) and its significance (b) for the pre-season T2 during 2001–2015.

Author Contributions: Conceptualization and formal analysis: L.G., J.G., S.W. and X.X.; Methodology, data curation and writing: C.H., L.Z. and L.G.

Funding: This work was funded by the National Natural Science Foundation of China (No. 41601580, 41671098), PhD Foundation of Henan University of Technology (No. B2015-17), Strategic Priority Research Program of the Chinese Academy of Sciences, (No. XDA19040304), Innovative research team of Henan Polytechnic University (No. T2018-4) and Open Foundation of Key Laboratory of Land Surface Pattern and Simulation, Chinese Academy of Sciences.

Acknowledgments: We also thank the journal editor and the anonymous reviewers for their useful comments and great efforts on this paper.

Conflicts of Interest: The authors declare no conflict of interest.

References

1. Tao, F.L.; Zhang, Z.; Zhang, S.; Rötter, R.P. Heat stress impacts on wheat growth and yield were reduced in the Huang–Huai–Hai Plain of China in the past three decades. *Eur. J. Agron.* **2015**, *71*, 44–52. [[CrossRef](#)]
2. Chen, X.L.; Liu, X.J.; Liu, L.T.; Zhang, Y.L.; Guo, J.H.; Huang, J.; Zhou, M.J.; Zhao, Y.; Wu, L.; Yang, L.; et al. Domestic Wheat Trade and Its Associated Virtual Cropland Flow in China, 2010–2015. *Sustainability* **2018**, *10*, 1459. [[CrossRef](#)]
3. Food and Agriculture Organization of the United Nations. Available online: <http://www.fao.org/home/en/> (accessed on 08 March 2019).
4. Chen, C.; Wang, E.L.; Yu, Q.; Zhang, Y.Q. Quantifying the effects of climate trends in the past 43 years (1961–2003) on crop growth and water demand in the North China Plain. *Clim. Chang.* **2010**, *100*, 559–578. [[CrossRef](#)]
5. Gao, J.B.; Jiao, K.W.; Wu, S.H.; Ma, D.Y.; Zhao, D.S.; Yin, Y.H.; Dai, E.F. Past and future effects of climate change on spatially heterogeneous vegetation activity in China. *Earth's Future* **2017**, *5*, 679–692. [[CrossRef](#)]
6. Ma, D.Y.; Deng, H.Y.; Yin, Y.H.; Wu, S.H.; Zheng, D. Sensitivity of arid/humid patterns in China to future climate change under a high-emissions scenario. *J. Geogr. Sci.* **2019**, *29*, 29–48. [[CrossRef](#)]
7. Zhang, H.L.; Zhao, X.; Yin, X.G.; Liu, S.L.; Xue, J.F.; Wang, M.; Pu, C.; Lai, R.; Chen, F. Challenges and adaptations of farming to climate change in the North China Plain. *Clim. Chang.* **2015**, *129*, 213–224. [[CrossRef](#)]

8. Fang, J.Y.; Yu, G.R.; Liu, L.L.; Hu, S.J.; Chapin, F.S. Climate change, human impacts, and carbon sequestration in China. *Proc. Natl. Acad. Sci. USA* **2018**, *115*, 4015–4020. [[CrossRef](#)]
9. Duo, A.; Zhao, W.J.; Qu, X.Y.; Jing, R.; Xiong, K. Spatio-temporal variation of vegetation coverage and its response to climate change in North China plain in the last 33 years. *Int. J. Appl. Earth Obs. Geoinf.* **2016**, *53*, 103–117. [[CrossRef](#)]
10. Wang, J.; Wang, E.L.; Yang, X.G.; Zhang, F.S.; Yin, H. Increased yield potential of wheat–maize cropping system in the North China Plain by climate change adaptation. *Clim. Chang.* **2012**, *113*, 825–840. [[CrossRef](#)]
11. Zhai, S.Y.; Song, G.X.; Qin, Y.C.; Ye, X.Y.; Lee, J. Modeling the impacts of climate change and technical progress on the wheat yield in inland China: An autoregressive distributed lag approach. *PLoS ONE* **2017**, *12*, e184474. [[CrossRef](#)]
12. Liu, Y.J.; Chen, Q.M.; Ge, Q.S.; Dai, J.H. Spatiotemporal differentiation of changes in wheat phenology in China under climate change from 1981 to 2010. *Sci. China Earth Sci.* **2018**, *61*, 1088–1097. [[CrossRef](#)]
13. Tao, F.L.; Zhang, S.; Zhang, Z. Spatiotemporal changes of wheat phenology in China under the effects of temperature, day length and cultivar thermal characteristics. *Eur. J. Agron.* **2012**, *43*, 201–212. [[CrossRef](#)]
14. Xiao, D.P.; Tao, F.L. Contributions of cultivars, management and climate change to winter wheat yield in the North China Plain in the past three decades. *Eur. J. Agron.* **2014**, *52*, 112–122. [[CrossRef](#)]
15. Li, K.N.; Yang, X.G.; Tian, H.Q.; Pan, S.F.; Liu, Z.J.; Lu, S. Effects of changing climate and cultivar on the phenology and yield of winter wheat in the North China Plain. *Int. J. Biometeorol.* **2016**, *60*, 21–32. [[CrossRef](#)] [[PubMed](#)]
16. Nguy–Robertson, A.; Suyker, A.; Xiao, X.M. Modeling gross primary production of maize and soybean croplands using light quality, temperature, water stress, and phenology. *Agric. Meteorol.* **2015**, *213*, 160–172. [[CrossRef](#)]
17. Wang, J.; Wu, C.Y.; Zhang, C.H.; Ju, W.M.; Wang, X.Y.; Chen, Z.; Fang, B. Improved modeling of gross primary productivity (GPP) by better representation of plant phenological indicators from remote sensing using a process model. *Ecol. Indic.* **2018**, *88*, 332–340. [[CrossRef](#)]
18. Han, Q.F.; Wang, T.J.; Jiang, Y.B.; Fischer, R.; Li, C.F. Phenological variation decreased carbon uptake in European forests during 1999–2013. *For. Ecol. Manag.* **2018**, *427*, 45–51. [[CrossRef](#)]
19. Zhou, L.; He, H.L.; Sun, X.M.; Zhang, L.; Yu, G.R.; Ren, X.L.; Wang, J.Y.; Zhao, F.H. Modeling winter wheat phenology and carbon dioxide fluxes at the ecosystem scale based on digital photography and eddy covariance data. *Ecol. Inform.* **2013**, *18*, 69–78. [[CrossRef](#)]
20. Xiao, D.P.; Tao, F.L.; Liu, Y.J.; Shi, W.J.; Wang, M.; Liu, F.S.; Zhang, S.; Zhu, Z. Observed changes in winter wheat phenology in the North China Plain for 1981–2009. *Int. J. Biometeorol.* **2013**, *57*, 275–285. [[CrossRef](#)]
21. Tao, F.L.; Zhang, Z.; Xiao, D.P.; Zhang, S.; Rötter, R.P.; Shi, W.J.; Liu, Y.J.; Wang, M.; Liu, F.S.; Zhang, H. Responses of wheat growth and yield to climate change in different climate zones of China, 1981–2009. *Agric. For. Meteorol.* **2014**, *189–190*, 91–104. [[CrossRef](#)]
22. He, L.; Asseng, S.; Zhao, G.; Wu, D.R.; Yang, X.Y.; Zhuang, W.; Jin, N.; Yu, Q. Impacts of recent climate warming, cultivar changes, and crop management on winter wheat phenology across the Loess Plateau of China. *Agric. For. Meteorol.* **2015**, *200*, 135–143. [[CrossRef](#)]
23. Wang, S.S.; Mo, X.G.; Liu, Z.J.; Baig, M.H.A.; Chi, W.F. Understanding long-term (1982–2013) patterns and trends in winter wheat spring green-up date over the North China Plain. *Int. J. Appl. Earth. Obs. Geoinf.* **2017**, *57*, 235–244. [[CrossRef](#)]
24. Cong, N.; Piao, S.L.; Chen, A.P.; Wang, X.H.; Lin, X.; Chen, S.P.; Han, S.J.; Zhou, G.S.; Zhang, X.P. Spring vegetation green-up date in China inferred from SPOT NDVI data: A multiple model analysis. *Agric. For. Meteorol.* **2012**, *165*, 104–113. [[CrossRef](#)]
25. Lu, L.L.; Wang, C.Z.; Guo, H.D.; Li, Q.T. Detecting winter wheat phenology with SPOT-VEGETATION data in the North China Plain. *Geocarto Int.* **2014**, *29*, 244–255. [[CrossRef](#)]
26. Guo, L.; An, N.; Wang, K.C. Reconciling the discrepancy in ground-and satellite-observed trends in the spring phenology of winter wheat in China from 1993 to 2008. *J. Geophys. Res. Atmos.* **2016**, *121*, 1027–1042. [[CrossRef](#)]
27. Liu, Z.J.; Wu, C.Y.; Liu, Y.S.; Wang, X.Y.; Fang, B.; Yuan, W.P.; Ge, Q.S. Spring green-up date derived from GIMMS3g and SPOT-VGT NDVI of winter wheat cropland in the North China Plain. *ISPRS J. Photogramm. Remote Sens.* **2017**, *130*, 81–91. [[CrossRef](#)]

28. Wang, D.; Fang, S.H.; Yang, Z.Z.; Wang, L.; Tang, W.C.; Li, Y.C.; Tong, C.Y. A Regional Mapping Method for Oilseed Rape Based on HSV Transformation and Spectral Features. *Int. J. Geo-Inf.* **2018**, *7*, 224. [[CrossRef](#)]
29. Tao, F.L.; Xiao, D.P.; Zhang, S.; Zhang, Z.; Rötter, R.P. Wheat yield benefited from increases in minimum temperature in the Huang–Huai–Hai Plain of China in the past three decades. *Agric. For. Meteorol.* **2017**, *239*, 1–14. [[CrossRef](#)]
30. Zheng, C.Y.; Zhang, J.; Chen, J.; Chen, C.Q.; Tian, Y.L.; Deng, A.X.; Song, Z.W.; Nawaz, M.M.; Groenigen, K.J.V.; Zhang, W.J. Nighttime warming increases winter–sown wheat yield across major Chinese cropping regions. *Field Crop. Res.* **2017**, *214*, 202–210. [[CrossRef](#)]
31. Shen, M.G.; Piao, S.L.; Chen, X.Q.; An, S.; Fu, Y.S.H.; Wang, S.P.; Cong, N.; Janssens, I.A. Strong impacts of daily minimum temperature on the green–up date and summer greenness of the Tibetan Plateau. *Glob. Chang. Biol.* **2016**, *22*, 3057–3066. [[CrossRef](#)]
32. Piao, S.L.; Tan, J.G.; Chen, A.P.; Fu, Y.S.H.; Ciais, P.; Liu, Q.; Janssens, I.A.; Vicca, A.; Zeng, Z.Z.; Jeong, S.J.; et al. Leaf onset in the northern hemisphere triggered by daytime temperature. *Nat. Commun.* **2015**, *6*, 6911. [[CrossRef](#)] [[PubMed](#)]
33. Shen, X.J.; Liu, B.H.; Henderson, M.; Wang, L.; Wu, Z.F.; Wu, H.T.; Jiang, M.; Lu, X.G. Asymmetric effects of daytime and nighttime warming on spring phenology in the temperate grasslands of China. *Agric. For. Meteorol.* **2018**, *259*, 240–249. [[CrossRef](#)]
34. Meng, Q.F.; Sun, Q.P.; Chen, X.P.; Cui, Z.L.; Yue, S.C.; Zhang, F.S.; Römheld, V. Alternative cropping systems for sustainable water and nitrogen use in the North China Plain. *Agric. Ecosyst. Environ.* **2012**, *146*, 93–102. [[CrossRef](#)]
35. Viovy, N.; Arino, O.; Belward, A.S. The Best Index Slope Extraction (BISE): A method for reducing noise in NDVI time–series. *Int. J. Remote Sens.* **1992**, *13*, 1585–1590. [[CrossRef](#)]
36. Zhang, Y.; Xiao, X.M.; Wu, X.C.; Zhou, S.; Zhang, G.L.; Qin, Y.W.; Dong, J.W. A global moderate resolution dataset of gross primary production of vegetation for 2000–2016. *Sci. Data* **2017**, *4*, 170165. [[CrossRef](#)]
37. Wang, J.; Xiao, X.M.; Zhang, Y.; Qin, Y.W.; Doughty, R.B.; Wu, X.C.; Bajgain, R.; Du, L. Enhanced gross primary production and evapotranspiration in juniper–encroached grasslands. *Glob. Chang. Biol.* **2018**, *24*, 5655–5667. [[CrossRef](#)]
38. Doughty, R.; Xiao, X.M.; Wu, X.C.; Zhang, Y.; Bajgain, R.; Zhou, Y.T.; Qin, Y.W.; Zou, Z.H.; McCarthy, H.; Friedman, J.; et al. Responses of gross primary production of grasslands and croplands under drought, pluvial, and irrigation conditions during 2010–2016, Oklahoma, USA. *Agric. Water Manag.* **2018**, *204*, 47–59. [[CrossRef](#)]
39. Resource and Environment Data Cloud Platform. Available online: <http://www.igsnrr.cas.cn> (accessed on 25 March 2019).
40. National Meteorological Information Center. Available online: <http://data.cma.cn/> (accessed on 25 March 2019).
41. Piao, S.L.; Fang, J.Y.; ZHOU, L.M.; Ciais, P.; Zhu, B. Variations in satellite–derived phenology in China’s temperate vegetation. *Glob. Chang. Biol.* **2006**, *12*, 672–685. [[CrossRef](#)]
42. Jeong, S.J.; Ho, C.H.; Gim, H.J.; Brown, M.E. Phenology shifts at start vs. end of growing season in temperate vegetation over the Northern Hemisphere for the period 1982–2008. *Glob. Chang. Biol.* **2011**, *17*, 2385–2399. [[CrossRef](#)]
43. Xu, Q.Y.; Yang, G.J.; Long, L.H.; Wang, C.C.; Li, X.C.; Huang, D.C. Crop information identification based on MODIS NDVI time–series data. *Trans. Chin. Soc. Agric. Eng.* **2014**, *30*, 134–144. (In Chinese) [[CrossRef](#)]
44. Wang, X.; Li, X.B.; Tan, M.H.; Xin, L.J. Remote sensing monitoring of changes in winter wheat area in North China Plain from 2001 to 2011. *Trans. Chin. Soc. Agric. Eng.* **2015**, *31*, 190–199. (In Chinese) [[CrossRef](#)]
45. Jiang, Y.Z.; Zhang, Y.J.; Sun, C.; You, S.C. MODIS–EVI based winter wheat planting information extraction of zoning on Huanghuaihai Plain. *Resour. Sci.* **2015**, *37*, 0417–0424. (In Chinese)
46. Dong, J.W.; Xiao, X.M.; Menarguez, M.A.; Zhang, G.L.; Qin, Y.W.; Thau, D.; Biradare, C.; Moore, B., III. Mapping paddy rice planting area in northeastern Asia with Landsat 8 images, phenology–based algorithm and Google Earth Engine. *Remote Sens. Environ.* **2016**, *185*, 142–154. [[CrossRef](#)] [[PubMed](#)]
47. Hou, X.H.; Gao, S.; Niu, Z.; Xu, Z.G. Extracting grassland vegetation phenology in North China based on cumulative SPOT–VEGETATION NDVI data. *Int. J. Remote Sens.* **2014**, *35*, 3316–3330. [[CrossRef](#)]

48. Shen, M.G.; Zhang, G.X.; Cong, N.; Wang, S.P.; Kong, W.D.; Piao, S.L. Increasing altitudinal gradient of spring vegetation phenology during the last decade on the Qinghai–Tibetan Plateau. *Agric. For. Meteorol.* **2014**, *189*, 71–80. [[CrossRef](#)]
49. Wu, C.Y.; Hou, X.H.; Peng, D.L.; Gonsamo, A.; Xu, S.G. Land surface phenology of China’s temperate ecosystems over 1999–2013: Spatial–temporal patterns, interaction effects, covariation with climate and implications for productivity. *Agric. For. Meteorol.* **2016**, *216*, 177–187. [[CrossRef](#)]
50. Zhao, W.Q.; Zhao, X.; Zhou, T.; Wu, D.H.; Tang, B.J.; Wei, H. Climatic factors driving vegetation declines in the 2005 and 2010 Amazon droughts. *PLoS ONE* **2017**, *12*, e175379. [[CrossRef](#)]
51. Wu, D.H.; Zhao, X.; Liang, S.L.; Zhou, T.; Huang, K.C.; Tang, B.J.; Zhao, W.Q. Time–lag effects of global vegetation responses to climate change. *Glob. Chang. Biol.* **2015**, *21*, 3520–3531. [[CrossRef](#)] [[PubMed](#)]
52. Wen, Y.Y.; Liu, X.P.; Xin, Q.C.; Wu, J.; Xu, X.C.; Pei, F.S.; Li, X.; Du, G.M.; Cai, Y.L.; Lin, K.; et al. Cumulative Effects of Climatic Factors on Terrestrial Vegetation Growth. *J. Geophys. Res. Biogeosci.* **2019**, *124*, 789–806. [[CrossRef](#)]
53. Lobell, D.B.; Field, C.B. Global scale climate–crop yield relationships and the impacts of recent warming. *Environ. Res. Lett.* **2007**, *2*, 14002. [[CrossRef](#)]
54. Zhang, Z.; Song, X.; Tao, F.L.; Zhang, S.; Shi, W.J. Climate trends and crop production in China at county scale, 1980 to 2008. *Theor. Appl. Climatol.* **2016**, *123*, 291–302. [[CrossRef](#)]
55. Wang, S.Y.; Yang, B.J.; Yang, Q.C.; Lu, L.L.; Wang, X.Y.; Peng, Y.Y. Temporal trends and spatial variability of vegetation phenology over the Northern Hemisphere during 1982–2012. *PLoS ONE* **2016**, *11*, e157134. [[CrossRef](#)] [[PubMed](#)]
56. Zhou, L.M.; Tucker, C.J.; Kaufmann, R.K.; Slayback, D.; Shabanov, N.V.; Myneni, R.B. Variations in northern vegetation activity inferred from satellite data of vegetation index during 1981 to 1999. *J. Geophys. Res. Atmos.* **2001**, *106*, 20069–20083. [[CrossRef](#)]
57. Cane, M.A. Climate science: Decadal predictions in demand. *Nat. Geosci.* **2010**, *3*, 231. [[CrossRef](#)]
58. Guemas, V.; Doblas–Reyes, F.J.; Andreu–Burillo, I.; Asif, M. Retrospective prediction of the global warming slowdown in the past decade. *Nat. Clim. Chang.* **2013**, *3*, 649–653. [[CrossRef](#)]
59. Li, Q.X.; Yang, S.; Xu, W.H.; Wang, X.L.; Jones, P.; Parker, D.; Zhou, L.M.; Feng, Y.; Gao, Y. China experiencing the recent warming hiatus. *Geophys. Res. Lett.* **2015**, *42*, 889–898. [[CrossRef](#)]
60. Fu, Y.H.; Zhao, H.F.; Piao, S.L.; Peaucelle, M.; Peng, S.S.; Zhou, G.Y.; Ciais, P.; Huang, M.T.; Menzel, A.; Peñuelas, J.; et al. Declining global warming effects on the phenology of spring leaf unfolding. *Nature* **2015**, *526*, 104. [[CrossRef](#)]
61. Piao, S.L.; Liu, Z.; Wang, T.; Peng, S.S.; Ciais, P.; Huang, M.T.; Ahlstrom, A.; Burkhardt, J.F.; Chevallier, F.; Janssens, I.A.; et al. Weakening temperature control on the interannual variations of spring carbon uptake across northern lands. *Nat. Clim. Chang.* **2017**, *7*, 359. [[CrossRef](#)]
62. Tung, K.K.; Chen, X.Y. Understanding the Recent Global Surface Warming Slowdown: A Review. *Climate* **2018**, *6*, 82. [[CrossRef](#)]
63. Wang, C.Z.; Fritschi, F.B.; Stacey, G.; Yang, Z.W. Phenology–Based Assessment of Perennial Energy Crops in North American Tallgrass Prairie. *Ann. Assoc. Am. Geogr.* **2011**, *101*, 742–751. [[CrossRef](#)]
64. Yu, H.Q.; Zhang, Q.; Sun, P.; Song, C.Q. Impact of Droughts on Winter Wheat Yield in Different Growth Stages during 2001–2016 in Eastern China. *Int. J. Disaster Risk Sci.* **2018**, *9*, 376–391. [[CrossRef](#)]
65. Anderson, L.O.; Malhi, Y.; Aragaõ, L.E.O.C.; Ladle, R.; Arai, E.; Barbier, N.; Phillips, O. Remote sensing detection of droughts in Amazonian forest canopies. *New Phytol.* **2010**, *187*, 733–750. [[CrossRef](#)] [[PubMed](#)]
66. Hua, W.J.; Chen, H.S.; Zhou, L.M.; Xie, Z.H.; Qin, M.H.; Li, X.; Ma, H.D.; Huang, Q.H.; Sun, S.L. Observational Quantification of Climatic and Human Influences on Vegetation Greening in China. *Remote Sens.* **2017**, *9*, 425. [[CrossRef](#)]
67. Tei, S.; Sugimoto, A. Time lag and negative responses of forest greenness and tree growth to warming over circumboreal forests. *Glob. Chang. Biol.* **2018**, *24*, 4225–4237. [[CrossRef](#)] [[PubMed](#)]
68. Cong, N.; Wang, T.; Nan, H.J.; Ma, Y.C.; Wang, X.H.; Myneni, R.B.; Piao, S.L. Changes in satellite–derived spring vegetation green–up date and its linkage to climate in China from 1982 to 2010: A multimethod analysis. *Glob. Chang. Biol.* **2013**, *19*, 881–891. [[CrossRef](#)] [[PubMed](#)]
69. Richardson, A.D.; Keenan, T.F.; Migliavacca, M.; Ryu, Y.; Sonnentag, O.; Toomey, M. Climate change, phenology, and phenological control of vegetation feedbacks to the climate system. *Agric. For. Meteorol.* **2013**, *169*, 156–173. [[CrossRef](#)]

70. Peng, S.S.; Piao, S.L.; Ciais, P.; Myneni, R.B.; Chen, A.P.; Chevallier, F.; Dolman, A.J.; Janssens, I.A.; Peñuelas, J.; Zhang, G.X. Asymmetric effects of daytime and night–time warming on Northern Hemisphere vegetation. *Nature* **2013**, *501*, 88–92. [[CrossRef](#)] [[PubMed](#)]
71. Pope, K.S.; Dose, V.; Da Silva, D.; Brown, P.B.; Leslie, C.A.; DeJong, T.M. Detecting nonlinear response of spring phenology to climate change by Bayesian analysis. *Glob. Chang. Biol.* **2013**, *19*, 1518–1525. [[CrossRef](#)]
72. Jeong, S.J.; Ho, C.H.; Kim, B.M.; Feng, S.; Medvigy, D. Non–linear response of vegetation to coherent warming over northern high latitudes. *Remote Sens. Lett.* **2013**, *4*, 123–130. [[CrossRef](#)]
73. Park, H.; Jeong, S.J.; Ho, C.H.; Kim, J.; Brown, M.E.; Schaepman, M.E. Nonlinear response of vegetation green–up to local temperature variations in temperate and boreal forests in the Northern Hemisphere. *Remote Sens. Environ.* **2015**, *165*, 100–108. [[CrossRef](#)]



© 2019 by the authors. Licensee MDPI, Basel, Switzerland. This article is an open access article distributed under the terms and conditions of the Creative Commons Attribution (CC BY) license (<http://creativecommons.org/licenses/by/4.0/>).